

1 Article

2 **Ni(NH<sub>3</sub>)<sub>2</sub>(NO<sub>3</sub>)<sub>2</sub> – A 3-D network through bridging nitrate units**  
3 **isolated from the thermal decomposition of nickel hexamine**  
4 **dinitrate.**

5 **Joachim Breternitz<sup>1,2</sup>, Agata Godula-Jopek<sup>3,4</sup> and Duncan H. Gregory<sup>1\*</sup>**

6 <sup>1</sup> WestCHEM School of Chemistry, University of Glasgow, University Avenue, G12 8QQ, Glasgow, UK;  
7 Duncan.Gregory@glasgow.ac.uk

8 <sup>2</sup> Helmholtz-Zentrum Berlin für Materialien und Energie, Department Structure and Dynamics of Energy  
9 Materials, Hahn-Meitner-Platz 1, 14109 Berlin, Germany; Joachim.Breternitz@helmholtz-berlin.de

10 <sup>3</sup> Airbus Group Innovations, XCXDI, 81663 Munich, Germany; agata.godula-jopek@airbus.com

11 <sup>4</sup> Institute of Chemical Engineering, Polish Academy of Sciences, 44100 Gliwice, Poland

12 \* Correspondence: Duncan.Gregory@glasgow.ac.uk; Tel.: +44-141-330-8128

13

14 **Abstract:** Nickel nitrate diammine, Ni(NH<sub>3</sub>)<sub>2</sub>(NO<sub>3</sub>)<sub>2</sub>, can be synthesised from the thermal  
15 decomposition of the nickel nitrate hexamine, Ni[(NH<sub>3</sub>)<sub>6</sub>](NO<sub>3</sub>)<sub>2</sub>. The hexamine decomposes in  
16 2 distinct steps; the first releases 4 equivalents of ammonia while the second involves the release of  
17 NO<sub>x</sub>, N<sub>2</sub> and H<sub>2</sub>O to yield NiO. The intermediate diammine compound can be isolated following  
18 the first deammoniation step or synthesised as a single phase from the hexamine under vacuum.  
19 Powder X-ray diffraction (PXRD) experiments have allowed the structure of Ni(NH<sub>3</sub>)<sub>2</sub>(NO<sub>3</sub>)<sub>2</sub> to be  
20 solved for the first time. The compound crystallises in orthorhombic space group *Pca*2<sub>1</sub> (*a* = 11.0628  
21 (5) Å, *b* = 6.0454 (3) Å, *c* = 9.3526 (4) Å; *Z* = 4) and contains 11 non-hydrogen atoms in the asymmetric  
22 unit. Fourier Transform Infrared (FTIR) spectroscopy demonstrates that the bonding in the ammine  
23 is consistent with the structure determined by PXD.

24 **Keywords:** crystal structure; ammine complex; structure determination; ammonia storage;  
25 vibrational spectroscopy.

26

---

27 **1. Introduction**

28 Ammonia is increasingly being considered as a safe, readily available alternative to hydrogen as  
29 an energy vector with an energy density of 13.6 GJ m<sup>-3</sup> (at 10 bar) [1] and the added advantage of  
30 possible storage at high gravimetric and volumetric capacities. Ammonia itself contains 17.6 wt%  
31 hydrogen and could be employed as a hydrogen carrier, releasing hydrogen *via* catalytic cracking.

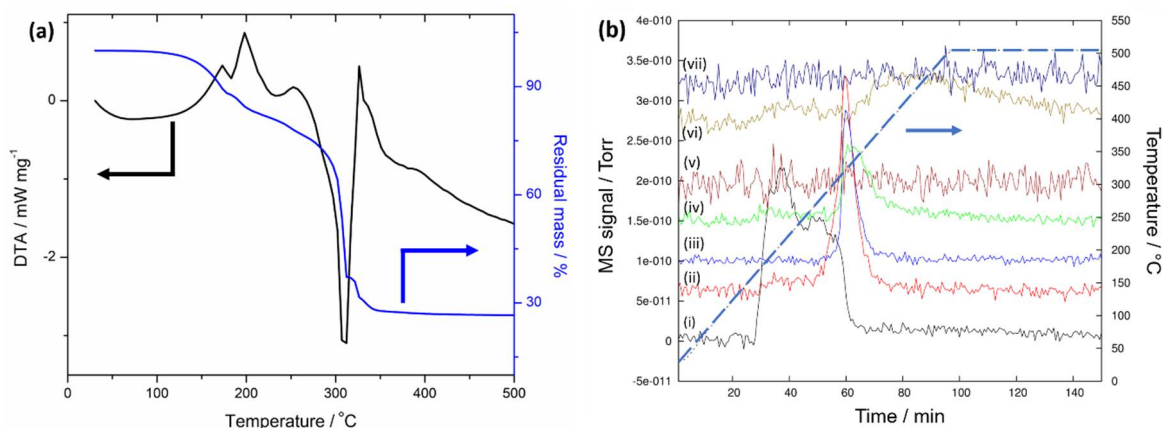
32 Metal ammine salts are attracting considerable interest as potential ammonia storage materials  
33 [2]. Transition metal salts readily form ammoniate complexes (ammines) with variable and  
34 controllable ammonia content [3]. The highest capacity (gravimetric density of ammonia) materials -  
35 typically hexamines - can be synthesised simply by the ambient temperature and pressure  
36 ammoniation of the respective transition metal salts. In an earlier study, we identified nickel salts as  
37 a promising group of ammonia storage materials [4]. Associated with this work, we were able to  
38 demonstrate that reaction of ammonia with nickel nitrate hexahydrate induces ligand exchange and  
39 the growth of nickel nitrate hexamine crystals [5]. The thermal decomposition of nickel nitrate  
40 hexamine has been discussed previously in the literature [6,7] and the products of the  
41 decomposition tentatively identified. The structure of the proposed thermodynamically stable  
42 intermediate decomposition product nickel diammine nitrate has remained unknown. In this work,  
43 we revisit the thermal decomposition of [Ni(NH<sub>3</sub>)<sub>6</sub>](NO<sub>3</sub>)<sub>2</sub> and determine the conditions for synthesis  
44 of the respective diammine Ni(NH<sub>3</sub>)<sub>2</sub>(NO<sub>3</sub>)<sub>2</sub>. The successful preparation of the compound as a single

45 phase has allowed us to determine its crystal structure for the first time and to perform a vibrational  
46 spectroscopy analysis of its bonding.

## 47 2. Results and Discussion

### 48 2.1. Thermal decomposition of $[\text{Ni}(\text{NH}_3)_6](\text{NO}_3)_2$

49



50 **Figure 1.** (a) Simultaneous thermal analysis of  $[\text{Ni}(\text{NH}_3)_6](\text{NO}_3)_2$  showing the thermogravimetric  
51 (blue) and differential thermal analysis (black) profiles. (b) Evolved gas analysis by mass spectrometry  
52 for (i)  $m/z = 17$  ( $\text{NH}_3^+$ , black), (ii)  $m/z = 28$  ( $\text{N}_2^+$ , red), (iii)  $m/z = 44$  ( $\text{N}_2\text{O}^+$ , blue), (iv)  $m/z = 30$  ( $\text{NO}^+$ ,  
53 green), (v)  $m/z = 46$  ( $\text{NO}_2^+$ , brown), (vi)  $m/z = 18$  ( $\text{H}_2\text{O}^+$ , olive) and (vii)  $m/z = 2$  ( $\text{H}_2^+$ , navy). The baselines  
54 are displaced along the y-axis for better visibility. The corresponding temperature is given by the  
55 dotted line.

56 The nickel hexammine,  $[\text{Ni}(\text{NH}_3)_6](\text{NO}_3)_2$ , was prepared using our previously published method  
57 and its complete characterisation is discussed therein [5].  $[\text{Ni}(\text{NH}_3)_6](\text{NO}_3)_2$  was studied by  
58 simultaneous thermal analysis that combined thermogravimetry (TG), differential thermal analysis  
59 (DTA) and evolved gas analysis by mass spectrometry (MS) in the same experiment (Figure 1). The  
60 thermal decomposition of the material is evidently complex and clear steps are, especially at higher  
61 temperatures, hard to distinguish. Considering the evolved gas mass spectra (Figure 1b), the initial  
62 decomposition that occurs below approximately 200 °C can be attributed exclusively to loss of  
63 ammonia, but not all the ammonia ligands are apparently removed before further decomposition  
64 products (from the decomposition of the nitrate anion) are detected. Therefore, the continued mass  
65 loss from the sample in the region of 200 - 300 °C must be interpreted in terms of simultaneous loss  
66 of further ammonia from the ammine complex in addition to nitrogen and nitrous oxides from the  
67 nitrate anions. From the identity of the evolved gases in the mass spectra, there is evidently reaction  
68 between fragments from the ammonia ligands and nitrate anion. It is interesting that no ammonia  
69 evolution is detected at temperatures above 300 °C, where  $\text{N}_2$ ,  $\text{N}_2\text{O}$ ,  $\text{NO}$  and  $\text{H}_2\text{O}$  prevail. Ultimately  
70 only  $\text{H}_2\text{O}$  is released at high temperature. These observed gaseous products match well to those  
71 observed previously for the decomposition of the hexammine nitrate in either argon or helium [6, 7].

72 It could be concluded that  $[\text{Ni}(\text{NH}_3)_6](\text{NO}_3)_2$  firstly loses ammonia to form lower ammine  
73 complexes, before loss of the remaining ammonia molecules coincides with the decomposition of the  
74 nitrate anions into nitrogen and nitrous oxides. This would leave a solid product of nickel hydroxide,  
75  $\text{Ni}(\text{OH})_2$ , which itself further decomposes into nickel oxide with the loss of water (in the final step).  
76 The first decomposition mass loss (Table 1) of 11.8 % corresponds well to the theoretical mass loss for  
77 the formation of the hypothetical tetrammine nickel nitrate,  $[\text{Ni}(\text{NH}_3)_4](\text{NO}_3)_2$  (11.94 %). The second  
78 step, however, itself is not large enough to account for the formation of either the triammine or  
79 diammine nickel nitrate (theoretically 17.91 % and 23.88 % respectively). In fact, the three successive

80 endotherms observed in the DTA trace below 300 °C would suggest that 2, 1 and 1 equivalents of  
 81 ammonia are lost resulting in the formation of the diammine and the weight loss by the end of the  
 82 third endotherm (of *ca.* 23 wt%) corresponds well to this assumption, even though the mass is not  
 83 constant at this point. There is thus no clear endpoint after the ammonia release and the sharp change  
 84 in slope of the mass loss likely originates from the immediate onset of nitrate anion decomposition  
 85 close to 300 °C. Steps 3 and 4 lie rather close to the expected mass losses for the formation of Ni(OH)<sub>2</sub>  
 86 (67.44 %) and NiO (73.77 %) and hence underline the decomposition of the nitrate anion at higher  
 87 temperatures. Given these results (most notably the DTA and MS data), we decided to use 200 °C as  
 88 the lowest possible temperature for the formation of the diammine nickel nitrate while avoiding the  
 89 decomposition of the nitrate anions. To drive the ammonia desorption, we performed the thermal  
 90 treatment under mild dynamic vacuum to facilitate the removal of ammonia from the system.

91 **Table 1.** TG-STA-MS analysis results for [Ni(NH<sub>3</sub>)<sub>6</sub>](NO<sub>3</sub>)<sub>2</sub>.

Step	Cumulative mass change / %	TG Temperatures / °C		DTA peak temperatures / °C	Gases evolved (from MS)
		Onset	Final		
1	-11.8	107	179	173	NH <sub>3</sub>
2	-16.9	187	208	198	NH <sub>3</sub>
3	-23.4	208	262	257	NH <sub>3</sub>
4	-63.1	272	316	309	NH <sub>3</sub> , N <sub>2</sub> , N <sub>2</sub> O, NO
5	-72.7	321	375	336	H <sub>2</sub> O

92

### 93 2.2. Crystal structure solution of Ni(NH<sub>3</sub>)<sub>2</sub>(NO<sub>3</sub>)<sub>2</sub>

94 When assessing the powder X-ray diffraction pattern of the thermal decomposition product, it  
 95 showed sharp reflections, but bore no similarities to previously described crystal structures in the  
 96 system. Attempts to automatically index the pattern using the programs Ito [8], Treor [9], Dicvol [10]  
 97 and McMaille [11] were successful and yielded consistent results, giving an orthorhombic cell with *a*  
 98  $\approx 11.1$  Å, *b*  $\approx 6.0$  Å and *c*  $\approx 9.4$  Å. In our experience, the use of more than one indexing program greatly  
 99 increases the confidence of the found solutions and can help to detect potential supercell solutions.

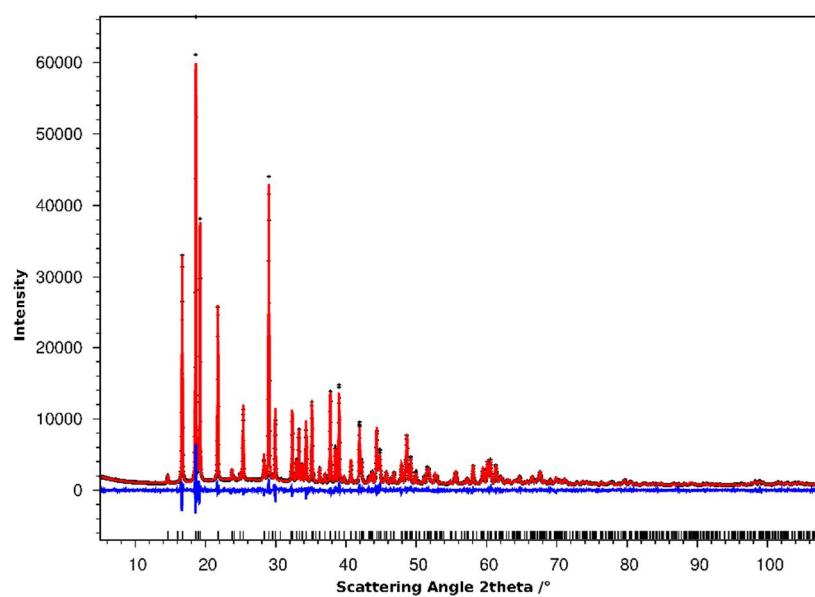
100 Following successful indexing, the pattern was treated using Jana2006 [12] and a sequence of Le  
 101 Bail fitting without symmetry assumptions (in space group *P*1), preliminary space group assignment  
 102 and Le Bail fitting in the assigned symmetry was performed. The structure solution was performed  
 103 *via* the Superflip routine [13] with subsequent Rietveld refinement both within Jana2006 (Table 2,  
 104 Figure 2). Given the limitations of powder X-ray diffraction in the accurate refinement of lighter atom  
 105 parameters, the thermal ellipsoids were modeled isotropically. The thermal parameters for N1 and  
 106 N2 (the crystallographically inequivalent nitrogen atoms in the ammonia molecules) were  
 107 constrained to equal values, as were those of O21 and O22 (bridging oxygen atoms within one of the  
 108 two inequivalent nitrate groups). The hydrogen atoms of the ammonia molecules were modelled as  
 109 riding on the nitrogen atoms and their *U*<sub>iso</sub> was constrained to be 1.2 times the *U*<sub>iso</sub> of the N atoms (as  
 110 suggested by Jana2006).

111

**Table 2.** Refinement Details for Ni(NH<sub>3</sub>)<sub>2</sub>(NO<sub>3</sub>)<sub>2</sub>.

Chemical formula	Ni(NH <sub>3</sub> ) <sub>2</sub> (NO <sub>3</sub> ) <sub>2</sub>
Formula Weight	216.8
Crystal system	Orthorhombic
Spacegroup	<i>Pca</i> 2 <sub>1</sub> (No. 29)
<i>a</i> / Å	11.0628(5)
<i>b</i> / Å	6.0454(3)
<i>c</i> / Å	9.3526(4)
<i>V</i> / Å <sup>3</sup>	625.49(5)
<i>Z</i>	4
crystallographic density / g cm <sup>-3</sup>	2.3018
No of data, parameters	4120, 68
<i>R<sub>p</sub></i> ; <i>wR<sub>p</sub></i>	0.044; 0.060
<i>R<sub>obs</sub></i> ; <i>wR<sub>2</sub></i> (all)	0.033; 0.044

112



113

114

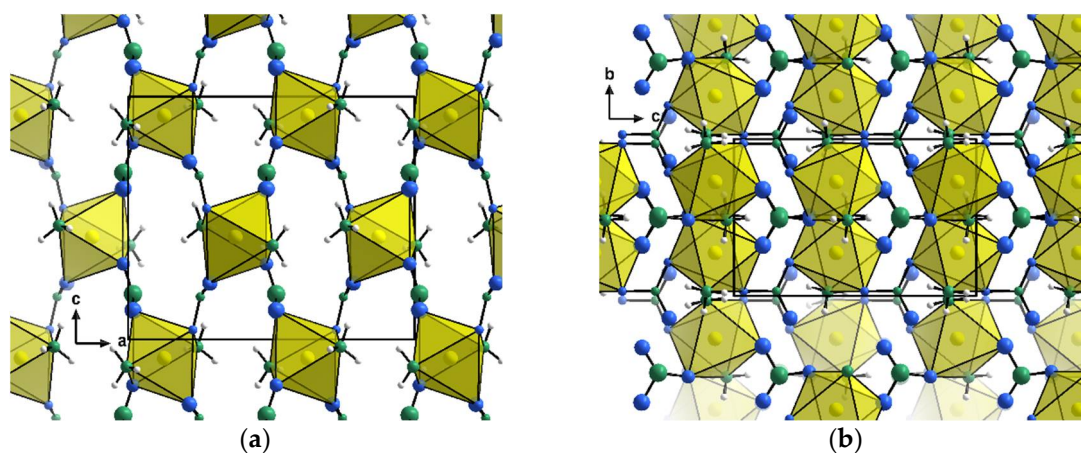
115

116

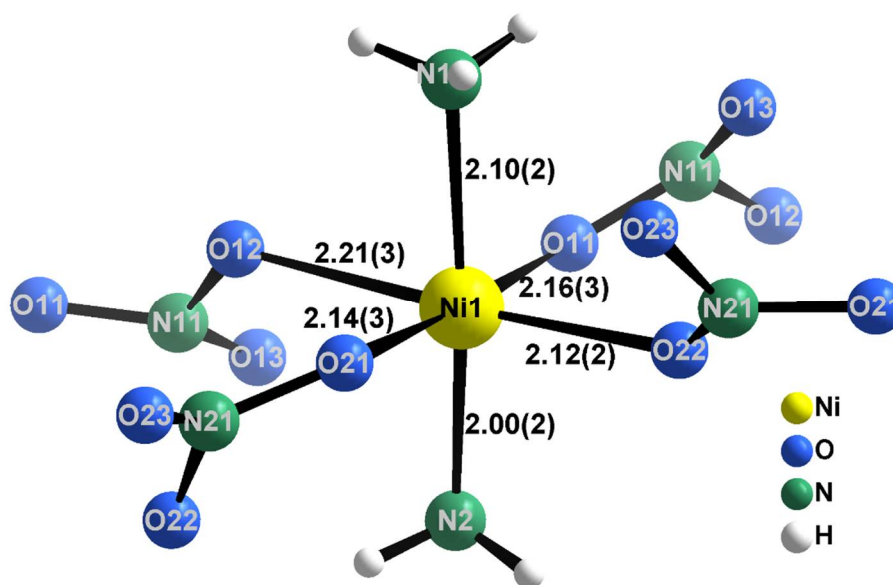
**Figure 2.** Plot of the measured powder pattern (black crosses) and calculated pattern (red line). The difference plot, ( $I_{\text{obs}} - I_{\text{calc}}$ ) is denoted by the blue line and the theoretical peak positions are shown as black ticks.

117 2.3. Crystal structure of  $\text{Ni}(\text{NH}_3)_2(\text{NO}_3)_2$ 

118  $\text{Ni}(\text{NH}_3)_2(\text{NO}_3)_2$  crystallises in the orthorhombic, non-centrosymmetric space group  $Pca2_1$  ( $a =$   
 119  $11.0628(5) \text{ \AA}$ ,  $b = 6.0454(3) \text{ \AA}$ ,  $c = 9.3526(4) \text{ \AA}$ ,  $V = 625.49(5) \text{ \AA}^3$ ) with eleven non-hydrogen atoms in the  
 120 asymmetric unit (Figure 3). The structure consists of a 3-dimensional network of compressed  
 121  $[\text{Ni}(\text{NH}_3)_2(\text{NO}_3)_2]$  octahedra, with the ammonia ligands trans- to one-another in the axial positions.  
 122 The octahedra are connected through four bridging nitrate anions per metal centre (and hence each  
 123 individual nitrate ligand bridges two metal centres, Figure 4). This structure type presents the first  
 124 evidence of bridging nitrate ligands in octahedral ammine complexes. In fact, the only other crystal  
 125 structures of ammine complexes containing nitrates as ligands are the copper nitrate di- and  
 126 monoammines [14] and platinum diammine dinitrate [15], where the nitrate and ammonia ligands  
 127 are coordinated to the metal centres in a square-planar geometry. Unlike these copper and platinum  
 128 compounds, which achieve three-dimensional connectivity through hydrogen bonds,  $\text{Ni}(\text{NH}_3)_2(\text{NO}_3)_2$   
 129 is connected in all 3 dimensions *via* bridging nitrate anions.  
 130



131 **Figure 3.** Representation of a unit cell of  $\text{Ni}(\text{NH}_3)_2(\text{NO}_3)_2$  along (a) the crystallographic  $b$ -direction  
 132 and (b) the crystallographic  $a$ -direction. Ni (gold), N (green) and O (blue) atoms are represented by  
 133 their thermal spheres at 90% probability, while H (white) atoms are given as generic balls.



134

135 **Figure 4.** Coordination sphere around the nickel centre (Ni1) in the crystal structure of  
 136  $\text{Ni}(\text{NH}_3)_2(\text{NO}_3)_2$ . The Ni-ligand distances are given in  $\text{ \AA}$ . Ni (gold), N (green) and O (blue) atoms are  
 137 represented by their thermal spheres at 90% probability, while H (white) atoms are given as generic  
 138 balls.

139

**Table 3.** Interatomic distances in Ni(NH<sub>3</sub>)<sub>2</sub>(NO<sub>3</sub>)<sub>2</sub>.

Atom 1	Atom 2	Distance / Å
<b>Nitrate bonds</b>		
N11	O11	1.23(6)
N11	O12	1.31(6)
N11	O13	1.16(6)
N21	O21	1.32(6)
N21	O22	1.25(4)
N21	O23	1.23(4)
<b>Nickel-ligand bonds</b>		
Ni1	N1	2.10(2)
Ni1	N2	2.00(2)
Ni1	O11	2.16(3)
Ni1	O12	2.21(3)
Ni1	O21	2.14(3)
Ni1	O22	2.12(2)

140

141

142

143

144

145

146

147

148

149

150

151

152

153

154

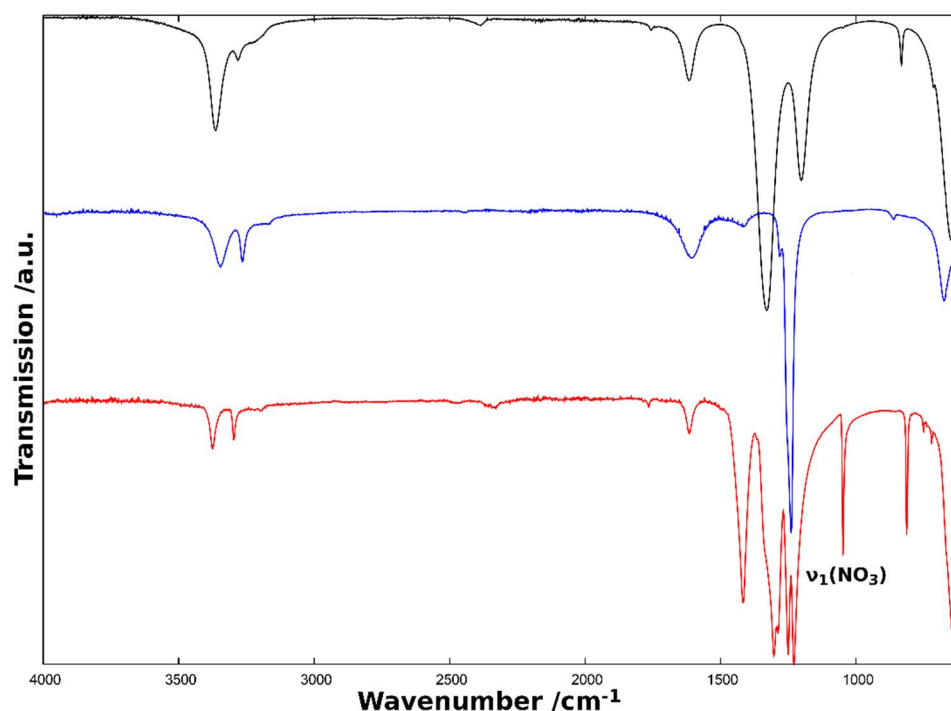
As expected from the presence of two different ligands in the first coordination sphere, the [Ni(NH<sub>3</sub>)<sub>2</sub>(NO<sub>3</sub>)<sub>4/2</sub>] octahedra are not regular (Figure 4, Table 3). The two Ni-N bonds are shorter (2.00(2) Å and 2.10(2) Å) than the equivalent Ni-O bonds (2.12(2) Å – 2.22(3) Å) and the angles deviate slightly from the ideal octahedral values, resulting in compressed octahedra along the axial direction. Further, the N-O distances in the nitrate anion are also strongly anisotropic and range from 1.16(6) Å - 1.32(6) Å. It is likely that the differences in the nitrate bond lengths are caused by comparatively strong hydrogen bonding interactions between the ammonia ligands and the terminal oxygen atoms in the nitrate anions (eight N-H...O hydrogen bonds with H...O ≤ 2.57 Å). The nitrate anion itself is also distorted in the plane of the nitrogen and oxygen atoms, departing from an ideal trigonal planar (D<sub>3h</sub>) geometry with out-of-plane torsion angles <(O11-O12-O13-N11) = -12(5)° and <(O21-O22-O23-N21) = -14(4)°. It should be noted that the relatively large errors on the values of these torsion angles suggest that the crystallographic evidence for the breaking of the D<sub>3h</sub> nitrate anion symmetry is not in itself incontrovertible. Breaking of the symmetry, be it through the torsion of the molecule or the bonding of oxygen atoms, is however sensitive to detection by IR spectroscopy.

155 2.4. IR spectroscopy of  $Ni(NH_3)_2(NO_3)_2$ 

156 The ammonia vibrational modes in diammine nickel nitrate are very similar to those in  
157 diammine nickel chloride and hexammine nickel nitrate (Figure 5, Table 3). A notable exception,  
158 however, is that the symmetric deformation band,  $\delta_s(HNH)$ , in hexammine nickel nitrate is split for  
159 the diammine compounds. This can be understood in terms of the more pronounced hydrogen  
160 bonding in the diammine complexes as compared to hexammine nickel nitrate. This is consistent with  
161 the symmetry inequivalence of the two ammonia ligands in  $Ni(NH_3)_2(NO_3)_2$  and hence supports the  
162 crystallographic model (where the two ammonia nitrogen positions are inequivalent).

163 Inclusion of nitrate anions within the first coordination sphere leads to an inevitable lowering of  
164 the molecular symmetry compared to the free nitrate anion [16] and hence leads to the appearance of  
165 further bands in the infrared spectrum [17]. Regarding the nitrate anion modes, several  
166 supplementary IR bands are observed in diammine nickel nitrate as compared to the equivalent  
167 hexammine (Figure 5). This can be attributed to the different bonding environments of the species.  
168 While the nitrate anion in hexammine nickel nitrate is not coordinated directly to the complex and  
169 therefore exists with ideal  $D_{3h}$  molecular symmetry, the same is not true for diammine nickel nitrate.  
170 The supplementary bands can be explained most clearly by comparison to the IR spectrum of  
171  $Ni(en)_2(NO_3)_2$  [17]. Most significantly, the appearance of the symmetric stretching mode ( $\nu_1$ ) at 1048  
172  $cm^{-1}$  is a clear and unambiguous indicator of the breaking of the ideal  $D_{3h}$  symmetry of the  $NO_3^-$   
173 anion. Whereas this mode is inactive for a trigonal species of  $D_{3h}$  symmetry (since the dipole moment does  
174 not change), it becomes active when the three-fold rotation axis is lost (resulting in either  $C_{2v}$  or  $C_s$   
175 symmetry). This occurs when the ligand is coordinated to a metal and the three nitrate oxygen atoms  
176 are no longer equivalent. Two further vibration modes that are degenerate for  $D_{3h}$  symmetry, the  
177 asymmetric stretching mode ( $\nu_3$ ) and the in-plane bending mode ( $\nu_4$ ), lose their degeneracy and are  
178 observed as separate bands in the IR spectrum of  $Ni(NH_3)_2(NO_3)_2$ . Furthermore, two sets of  
179 combination modes ( $\nu_1+\nu_3$  and  $\nu_1+\nu_4$ ) appear with the aforementioned fundamental modes and the  
180 supplementary out-of-plane mode  $\nu_2$ .

181



182

183 **Figure 5.** FTIR spectrum of  $Ni(NH_3)_2(NO_3)_2$  (red) in comparison with the spectra of  $Ni(NH_3)_2Cl_2$  [4]  
184 given in blue and  $Ni(NH_3)_6(NO_3)_2$  [5] given in black.

185

186  
187**Table 3.** Assignment of the infrared bands in Ni(NH<sub>3</sub>)<sub>2</sub>(NO<sub>3</sub>)<sub>2</sub> in comparison to the documented values of Ni(en)<sub>2</sub>(NO<sub>3</sub>)<sub>2</sub> [17], Ni(NH<sub>3</sub>)<sub>2</sub>Cl<sub>2</sub> [4] and Ni(NH<sub>3</sub>)<sub>6</sub>(NO<sub>3</sub>)<sub>2</sub> [5].

Band	Wavenumber / cm <sup>-1</sup>			
	Ni(NH <sub>3</sub> ) <sub>2</sub> (NO <sub>3</sub> ) <sub>2</sub>	Ni(en) <sub>2</sub> (NO <sub>3</sub> ) <sub>2</sub> [17]	Ni(NH <sub>3</sub> ) <sub>2</sub> Cl <sub>2</sub> [4]	Ni(NH <sub>3</sub> ) <sub>6</sub> (NO <sub>3</sub> ) <sub>2</sub> [5]
$\nu_a(\text{NH}_3)$	3375		3346	3364
$\nu_s(\text{NH}_3)$	3296		3265	3282
$2\delta_a(\text{HNNH})$	3195		3167	3167
$\nu_1+\nu_3(\text{NO}_3)$	2475	2455		
$\nu_1+\nu_3(\text{NO}_3)$	2330	2320		
$\nu_1+\nu_4(\text{NO}_3)$	1765	1762, 1741		
$\delta_a(\text{HNNH})$	1616		1607	1616
$\nu_3(\text{NO}_3)$	1417	1420		
$\nu_3(\text{NO}_3)$	1303	1303		1329
$\delta_s(\text{HNNH})$	1250		1281	
$\delta_s(\text{HNNH})$	1229		1239	1202
$\nu_1(\text{NO}_3)$	1048	1033, 1034		
$\nu_2(\text{NO}_3)$	812	818		823
$\nu_4(\text{NO}_3)$	751	728		
$\nu_4(\text{NO}_3)$	721	708		
$\rho(\text{NH}_3)$	643		675	648

188

189 **3. Materials and Methods**190 *3.1. Synthesis*

191 Ni(H<sub>2</sub>O)<sub>6</sub>(NO<sub>3</sub>)<sub>2</sub> (AnalaR – BDH Chemicals, 99 %) was used as supplied. The title compound was  
 192 synthesised through thermal decomposition of Ni(NH<sub>3</sub>)<sub>6</sub>(NO<sub>3</sub>)<sub>2</sub>, made from Ni(H<sub>2</sub>O)<sub>6</sub>(NO<sub>3</sub>)<sub>2</sub> as  
 193 described previously [5]. Ni(NH<sub>3</sub>)<sub>6</sub>(NO<sub>3</sub>)<sub>2</sub> was heated under mild dynamic vacuum (*ca.* 10<sup>-2</sup> bar) to

194 100 °C for 30 minutes in order to remove any remaining humidity from the compound. The complex  
195 was then further heated to 200 °C for 2 h under the same conditions to decompose the hexamine  
196 into the diammine. The completeness of the reaction could be followed by observing the change of  
197 the compound colour from purple to green.

### 198 3.2. Thermal analysis

199 Thermal analyses were conducted on a Netzsch 409 PC STA instrument under flowing argon  
200 gas (BOC, 99.998 %) coupled to a Hiden Analytical HPR 20 mass spectrometer. Combined STA-MS  
201 studies were conducted at a heating rate of 5 K min<sup>-1</sup>. The STA instrument was located inside an  
202 Argon filled glove box (UNIlab, MBraun) with O<sub>2</sub> and H<sub>2</sub>O levels below 3 ppm to avoid possible  
203 reactions of samples with moist air. The samples were loaded into Al<sub>2</sub>O<sub>3</sub> sample holders.

### 204 3.3. Fourier transform infrared (FTIR) spectroscopy

205 Infrared spectra were collected on an attenuated total reflection Fourier-transform infrared  
206 spectrometer (ATR-FTIR) in the wavenumber range of 4000–600 cm<sup>-1</sup> on an FTIR-8400S (Shimadzu).  
207 24 accumulated spectra were collected with a resolution of 2 cm<sup>-1</sup>.

### 208 3.4. Powder X-ray diffraction

209 Samples of the hexamine and diammine were loaded into glass capillaries (Hilgenberg, 0.7  
210 mm diameter) and flame-sealed. Samples was measured in Debye-Scherrer geometry on a Bruker D8  
211 Advance diffractometer with Cu-Kα<sub>1</sub> radiation (5° ≤ 2θ ≤ 108°, step size = 0.025°). Powder data were  
212 analysed as discussed in section 2.2.  
213

## 214 4. Conclusions

215 From an investigation of the thermal decomposition of Ni(NH<sub>3</sub>)<sub>6</sub>(NO<sub>3</sub>)<sub>2</sub> it was possible to  
216 determine the synthetic conditions required to isolate the diammine nickel nitrate, Ni(NH<sub>3</sub>)<sub>2</sub>(NO<sub>3</sub>)<sub>2</sub>.  
217 Subsequent synthesis enabled the phase-pure polycrystalline diammine to be obtained and structure  
218 solution to be performed from powder X-ray diffraction data. Ni(NH<sub>3</sub>)<sub>2</sub>(NO<sub>3</sub>)<sub>2</sub> crystallises in the  
219 orthorhombic space group *Pca*2<sub>1</sub> and forms a novel structure type in which Ni centres are  
220 octahedrally coordinated by ammonia and nitrate in axial and equatorial positions respectively. The  
221 latter ligands bridge to form a 3-dimensional network. Using vibrational spectroscopy, we could both  
222 substantiate the chemical inequivalence of the two trans-ammonia ligands and confirm the  
223 involvement of the nitrate groups as ligands *via* signature bands attributable to the breaking of the  
224 ideal D<sub>3h</sub> trigonal planar symmetry. Following similar strategies should facilitate the isolation and  
225 characterisation of further metal nitrate amines and clarify the reaction pathways involved in  
226 deammoniation.

227 **Supplementary Materials:** The following are available online at [www.mdpi.com/link](http://www.mdpi.com/link): cif-file for  
228 Ni(NH<sub>3</sub>)<sub>2</sub>(NO<sub>3</sub>)<sub>2</sub>.

229 **Acknowledgments:** D.H.G. thanks Airbus Group Innovations for funding a studentship for J.B.

230 **Author Contributions:** J.B. and D.H.G. conceived and designed the experiments; J.B. performed the experiments  
231 and analysed the data; J.B, A.G.J. and D.H.G. authored the paper. A.G.J and D.H.G supervised the research.

232 **Conflicts of Interest:** The authors declare no conflict of interest.

## 233 References

- 234 1. Zamfirescu, C.; Dincer, I. Using ammonia as sustainable fuel. *J. Power Sources* **2008**, *185*, 459-465,  
235 DOI:10.1016/j.jpowsour.2008.02.097.

- 236 2. Sørensen, R. Z.; Hummelshøj, J. S.; Klerke, A.; Reves, J. B.; Vegge, T.; Nørskov, J. K.; Christensen, C. H.  
237 Indirect, Reversible High-Density Hydrogen Storage in Compact Metal Ammine Salts. *J. Am. Chem. Soc.*  
238 **2008**, *130*, 8660–8668, DOI: 10.1021/ja076762c.
- 239 3. Reardon, H.; Hanlon, J. M.; Grant, M.; Fullbrook, I.; Gregory, D. H. Ammonia Uptake and Release in the  
240  $MnX_2-NH_3$  ( $X = Cl, Br$ ) Systems and Structure of the  $Mn(NH_3)_nX_2$  ( $n = 6, 2$ ) Ammines. *Crystals* **2012**, *2*, 193-  
241 212, DOI:10.3390/cryst2020193.
- 242 4. Breternitz, J.; Vilk, Y.E.; Giraud, E.; Reardon, H.; Hoang, T.K.A.; Godula-Jopek, A.; Gregory, D. H. Facile  
243 Uptake and Release of Ammonia by Nickel Halide Ammines. *ChemSusChem* **2016**, *9*, 312-321, DOI:  
244 10.1002/cssc.201600140.
- 245 5. Breternitz, J.; Farrugia, L.J.; Godula-Jopek, A.; Saremi-Yaramahdi, S.; Malka, I.E.; Hoang, T.K.A.; Gregory,  
246 D.H. Reaction of  $[Ni(H_2O)_6](NO_3)_2$  with gaseous  $NH_3$ ; crystal growth *via* in-situ solvation. *J. Cryst. Growth*  
247 **2015**, *412*, 1-6, DOI: 10.1016/j.jcrysgro.2014.11.021.
- 248 6. Migdał-Mikuli, A.; Mikuli, E.; Dziembaj, R.; Majda, D.; Hetmańczyk, Ł. Thermal decomposition of  
249  $[Mg(NH_3)_6](NO_3)_2$ ,  $[Ni(NH_3)_6](NO_3)_2$  and  $[Ni(ND_3)_6](NO_3)_2$ . *Thermochim. Acta* **2004**, *419*, 223–229, DOI:  
250 10.1016/j.tca.2004.01.035.
- 251 7. Mikuli, E.; Migdał-Mikuli, A.; Majda, D. Thermal decomposition of polycrystalline  $[Ni(NH_3)_6](NO_3)_2$ . *J.*  
252 *Therm. Anal. Calorim.* **2013**, *112*, 1191-1198, DOI: 10.1007/s10973-012-2640-8.
- 253 8. Visser, J. W. A fully automatic program for finding the unit cell from powder data. *J. Appl. Crystallogr.* **1969**,  
254 *2*, 89–95, DOI: 10.1107/S0021889869006649
- 255 9. Werner, P.-E.; Eriksson, L.; Westdahl, M. TREOR, a semi-exhaustive trial-and-error powder indexing  
256 program for all symmetries. *J. Appl. Crystallogr.* **1985**, *18*, 367–370, DOI: 10.1107/S0021889885010512.
- 257 10. Boultif, A.; Louër, D. Indexing of powder diffraction patterns for low-symmetry lattices by the successive  
258 dichotomy method. *J. Appl. Crystallogr.* **1991**, *24*, 987–993, DOI: 10.1107/S0021889891006441.
- 259 11. Le Bail, A. Monte carlo indexing with mcmaile. *Powder Diffr.* **2004**, *19*, 249–254, DOI: 10.1154/1.1763152.
- 260 12. Petříček, V.; Dušek, M.; Palatinus, L. Crystallographic Computing System JANA2006: General features. *Z.*  
261 *Kristallogr. - Cryst. Mater.* **2014**, *229*, 345–352, DOI: 10.1515/zkri-2014-1737.
- 262 13. Palatinus, L.; Chapuis, G. SUPERFLIP - a computer program for the solution of crystal structures by charge  
263 flipping in arbitrary dimensions. *J. Appl. Crystallogr.* **2007**, *40*, 786–790, DOI: 10.1107/S0021889807029238.
- 264 14. Morozov, I. V.; Korenev, Y. M.; Troyanov, S. I. Synthesis and crystal structure of New Amminecopper(II)  
265 Nitrates:  $[Cu(NH_3)_2](NO_3)_2$  and  $[Cu(NH_3)](NO_3)_2$ . *Z. Anorg. Allgem. Chem.* **1996**, *622*, 2003-2007, DOI:  
266 10.1002/zaac.19966221132.
- 267 15. Lippert, B.; Lock, C.; Rosenberg, B.; Zvagulis, M. cis-Dinitratodiammineplatinum(II), cis- $Pt(NH_3)_2(NO_3)_2$ .  
268 Crystalline structure and vibrational spectra. *Inorg. Chem.* **1977**, *16*, 1525–1529, DOI: 10.1021/ic50172a057.
- 269 16. Addison, C. C.; Logan, N.; Wallwork, S. C.; Garner, C. D. Structural aspects of co-ordinated nitrate groups.  
270 *Q. Rev., Chem. Soc.* **1971**, *25*, 289–322, DOI: 10.1039/QR9712500289.
- 271 17. Curtis, N. F.; Curtis, Y. M. Some Nitrate-Amine Nickel(II) Compounds with Monodentate and Bidentate  
272 Nitrate Ions. *Inorg. Chem.* **1965**, *4*, 804–809, DOI: 10.1021/ic50028a007.

273

274